



# A shear-enhanced CNT-assembly nanosensor platform for ultra-sensitive and selective protein detection

Diya Li, Ceming Wang, Gongchen Sun, Satyajyoti Senapati\*, Hsueh-Chia Chang\*

Department of Chemical and Biomolecular Engineering, University of Notre Dame, 321 Stinson Remick, Notre Dame, IN 46556, United States



## ARTICLE INFO

### Keywords:

Carbon nanotubes  
Nanowire assembly  
AC dielectrophoresis  
Electrochemical sensing  
Hydrodynamic shear

## ABSTRACT

Detection and quantification of low-concentration proteins in heterogeneous media are generally plagued by two distinct obstacles: lack of sensitivity due to high dissociation equilibrium constant  $K_D$  and non-specificity due to an abundance of non-targets with similar  $K_D$ . Herein, we report a nanoscale protein-sensing platform with a non-equilibrium on-off switch that employs dielectrophoretic and hydrodynamic shear forces to overcome these thermodynamic limitations with irreversible kinetics. The detection sensitivity is achieved with complete association of the antibody-antigen-antibody (Ab-Ag-Ab) complex by precisely and rapidly assembling carbon nanotubes (CNT) across two parallel electrodes *via* sequential DC electrophoresis and AC dielectrophoresis (DEP), and with single-CNT electron tunneling conductance. The high selectivity is achieved with a critical hydrodynamic shear rate between the activated dissociation shear rates of target and non-target linkers of the aligned CNTs. We are able to reach detection limits of 100 attomolar (aM) and 10 femtomolar (fM) in pure samples for two ELISA assays with low and high dissociation constant: biotin/streptavidin (10 fM) and HER2/HER2 antibody ( $0.44 \pm 0.07$  nM), respectively. For both models, irreversible capture and shearing allow us to tune the dynamic range up to 5 decades by increasing the CNT numbers. We also demonstrate in spiked serum sample high selectivity towards target HER2 proteins against non-target HER2 isoform of a similar  $K_D$ . The detection limit for HER2 in serum is lower than 100 fM.

## 1. Introduction

A sensitive, selective, rapid and affordable detection of proteins has potential applications in early detection (Kohno et al., 2011; Bruno and Njar, 2007; Anderson, 2005) and monitoring disease progressions (Kitano, 2002; Srinivas et al., 2001). Conventional gold standard assay for protein detection is the enzyme-linked immunosorbent assay (ELISA) (Jia et al., 2009; Findlay et al., 2000). But the assay lacks the requisite detection sensitivity for many clinical samples due to high dissociation constant  $K_D$  of most antibody-antigen pairs, rendering the antibody-antigen (Ab-Ag) complex thermodynamically unfavorable at target concentration lower than  $K_D$ . Since most antibodies have  $K_D$  in the low  $\mu\text{M}$  to  $\text{nM}$  range (Hu et al., 2007; Glaser, 1993), with a few high-affinity antibodies in the  $\text{pM}$  range, detections lower than  $\text{pM}$  are hence considered to be beyond reach. Furthermore, the detection dynamic range of ELISA is often 2–3 orders of magnitude as a result of target saturation at equilibrium (Gam, 2012). This low dynamic range of assays is incompatible with physiological protein concentrations that vary over 4 orders of magnitude in serum, blood or urine (Lilja et al., 2008; Rusling et al., 2010). Lack of selectivity is another

problem for the ELISA assay that leads to false positives. For instance, false positive detection of bladder cancer urinary protein biomarker can be as high as 31% (Budman et al., 2008). False positives are caused by non-targets with similar  $K_D$ , which cannot be removed by conventional washing steps during the assay. Even if there is a significant difference in  $K_D$  between targets and non-targets, the low-abundant targets cannot compete for the antibodies when the concentrations of the non-target proteins exceed that of the target by orders of magnitude (Hortin and Sviridov, 2010). Therefore, development of a generic protein detection platform that has high sensitivity, selectivity and large dynamic range would then allow detection and quantification of arbitrary protein targets in untreated physiological samples by current commercial antibodies.

The technical obstacles of ELISA assay for early disease detection, accurate prognosis and highly reliable predictions are pushing the biosensing community to come up with novel detection technologies to enhance detection sensitivity and selectivity (Kokkinos et al., 2016; Pei et al., 2013). The nanoscale electrochemical immunoassay opens new horizons for highly sensitive yet simple and robust detection of biomarkers (Zhu et al., 2015; Chikkaveeraiah et al., 2012; Privett

\* Corresponding authors.

E-mail addresses: [dli4@nd.edu](mailto:dli4@nd.edu) (D. Li), [cwang9@nd.edu](mailto:cwang9@nd.edu) (C. Wang), [gsun1@nd.edu](mailto:gsun1@nd.edu) (G. Sun), [ssenapat@nd.edu](mailto:ssenapat@nd.edu) (S. Senapati), [hchang@nd.edu](mailto:hchang@nd.edu) (H.-C. Chang).

et al., 2010; Grieshaber et al., 2008). In particular, CNT sensors provide a wide electrochemical window, fast electron transfer kinetics, and biocompatibility, which make them a good candidate for electrochemical molecular recognition (Balasubramanian and Burghard, 2006). A CNT-FET label-free protein biosensor was reported by Maehashi et al. (2007) with a detection limit down to 250 pM. The detection is quantified by measuring source-drain current of CNT-FET as it changes with protein docking on the antibodies or aptamers functionalized surface. More recently, Gomes-Filho et al. (2013) overcome the detection limitation for an antibody-functionalized CNT ELISA sensor by using an enzymatic amplification technique with horseradish peroxidase (HRP) conjugated detection antibodies. The amperometric signals are thus amplified under optimum pH and buffer concentration with a detection limit of 0.033 ng/ml (~1 pM). Pandiaraj et al. (2014) on the other hand, doped the system with redox species Fe (III)/Fe (II), which decreases the charge-transfer resistance  $R_{ct}$  to improve the sensitivity.

However, the CNT-FET charge sensor can only detect charged proteins within one Debye length from the surface of the CNT and is hence sensitive to the sample ionic strength (Stern et al., 2007). Even though enzymatic/redox-reporter amplifies current signal, those electroactive species activities are strongly influenced by the medium pH (Zhang et al., 2016), which may affect the conformations of target proteins and thus limits the detection sensitivity. Moreover, the stability of enzyme functionality and thermodynamic affinity of the enzyme-conjugated antibodies can potentially compromise the high CNT sensitivity. Therefore, a robust and selective CNT-ELISA platform that does not depend on medium pH, ionic strength and extensive sample pretreatment would significantly enhance the CNT platform.

We report such a platform here by significantly enhancing both the thermodynamic sensitivity and selectivity of the ELISA complex with non-equilibrium and irreversible phenomena related to CNTs. The CNTs are used as capturing, reporting and selectivity enhancement agents in conjunction with a precise but rapid assembly technique. The high aspect ratio of the CNT endows them with large induced dipoles (Zhou et al., 2007), large dielectrophoretic mobility (Zhou et al., 2006) and large hydrodynamic drag (Hölzer and Sommerfeld, 2008). After targets are introduced to bind with polyclonal capture antibodies on the parallel Au electrodes that are 1  $\mu$ m separated, a solution containing the monoclonal detection antibodies functionalized CNTs with wrapped DNAs are driven by DC electrophoresis and AC dielectrophoresis (DEP) to assemble across the electrode pair and form antigen-antibody-antigen (Ab-Ag-Ab) ELISA complex. The rapid and irreversible DC and AC DEP trapping not only captures more targets than is allowed by molecular association at equilibrium, but also significantly reduces the overall assay time compared to diffusion-limited assays. Zhou et al. (2006), Cheng et al. (2010) and Basuray et al. (2009) have proven that the high AC field at assembled CNTs across two parallel electrodes can rapidly isolate bacteria and long DNAs in a flowing solution by dielectrophoresis. Next, a cross-flow passes across the assembled CNTs to irreversibly shear off non-target-CNT complexes, thus enhancing the selectivity of the platform. Since the hydrodynamic drag force of CNTs is inversely proportional to the nature log of CNT's aspect ratio, the force is 2 orders of magnitude higher than that of a normal wash without CNTs. Thus, the force can be precisely tuned with shear rate to achieve the optimal selectivity for an Ab-Ag pair, as the CNTs are perfectly aligned in the assembly. Only target-CNTs complexes remain after shear, and the number of detectable targets is governed by the CNT number that can be easily tuned to produce a large dynamic range. As a result, we have developed a new robust CNT protein nanosensor platform that is simple and rapid, with high sensitivity and specificity over a 5-decade dynamic range.

## 2. Material and methods

### 2.1. Reagents and chemicals

Streptavidin, 11-Mercaptoundecanoic acid, 1X PBS (pH 7.4), EDC (1-ethyl-3-[3-dimethylaminopropyl]carbodiimide hydrochloride), human serum, and gold etchant were obtained from Sigma Aldrich. EZ-link amine-PEG<sub>2</sub>-Biotin was obtained from VWR, MES sodium salt was purchased from Fischer Scientific. HER2 protein, HER2 capture antibody, detection antibody, HER2 partial recombinant protein were purchased from Novus Biologicals. Single strand DNA was obtained from IDT (Integrated DNA Technologies) with a sequence of 5' TGG TTC TCT CCG AAA TAG CTT TAG GG of molecular weight is 8898.8 g/mol. COOH-SWCNTs was purchased from Carbon Solution. A dialysis kit was obtained from Thermo Scientific with a MWCO value of 7000. 54.59 mg of 11-mercaptoundecanoic acid was dissolved in 50 ml of 95% of alcohol solution to make a 5 mM of thiol solution, and the pH was adjusted to 2 with 0.1 M HCl. 0.1 M of MES (pH 5.5) was prepared by dissolving 10.861 g MES sodium salt in 500 ml of DI water, and the pH is adjusted with 0.5 M of NaOH. 100 mM of EDC solution was made by dissolving 19 mg EDC in 1 ml of MES solution, and 50 mM of biotin solution was prepared with 19 mg biotin in 1 ml of MES solution. Different concentrations of streptavidin, HER2 and negative control HER2 isoform were dissolved in 1X PBS. 10  $\mu$ l of 0.08  $\mu$ g/ $\mu$ l of HER2 was spiked into 490  $\mu$ l of human serum to make a 1 nM sample. The biotin solution was stored in a freezer at 4 °C until ready for use, and all streptavidin and HER2 samples were stored at -20 °C. The samples were slowly dissolved at 0 °C before use.

### 2.2. Fabrication of chip pattern with 1 $\mu$ m and 3 $\mu$ m gaps

Patterns were fabricated on glass slides that were first soaked in base piranha for 3 min and washed thoroughly with DI water. Detailed fabrication steps for chips with 3  $\mu$ m and 1  $\mu$ m gaps are discussed in the supplementary section (S.1a and S.2a).

### 2.3. Functionalization of biotin/capture HER2 antibody on gold electrode

Chips with 1  $\mu$ m wide gap were incubated in 5 mM thiol solution for 24 h after N<sub>2</sub> gas purging for 5 min to remove oxygen. Detailed techniques and results are discussed in the supplementary section (S.2b and Fig. S-2).

### 2.4. Dispersion of COOH-SWCNTs and functionalization of DNA and biotin/detection HER2 antibody on CNT surface

4 mg of COOH-SWCNTs with a length of 1–3  $\mu$ m were added into 6 ml of DI water and ultra-sonicated with 1 s pulse and 1 s rest for 5 min under 40% power (10 W) using Qsonica sonicators. The upper 1 ml solution was collected after ultra-centrifugation for 90 min at 18334g. Then, 40  $\mu$ l of the solution was mixed with 40  $\mu$ l of 1 mM ssDNA solution in 1X PBS under a light sonication at 20% power with 1 s pulse and 1 s rest for 5 min. After DNAs have non-specifically bound to CNTs, 10  $\mu$ l of EDC in MES solution was added to react with the DNA wrapped COOH-SWCNTs, and the solution was lightly sonicated at 20% power with 1 s pulse and 1 s rest for 5 min. To functionalize biotin onto COOH-SWCNTs, 10  $\mu$ l of 50 mM of biotin was then added to covalently bind with CNTs for 2 h and the solution was gently mixed with a rotator. At last, the solution was dialyzed to remove any non-bounded biotin and EDC for 6.5 h, and the collected solution was used as a biotin functionalized CNTs stock solution. To functionalize detection (monoclonal) HER2 antibody onto COOH-SWCNTs, 10  $\mu$ l of 0.05 mg/ml of monoclonal HER2 antibody in 1XPBS solution was added to covalently bind with CNTs for 2 h, and the solution was mixed with a rotator. At last, the solution was centrifuged at a speed of

13.3g for 5 min, and the supernatant was collected as HER2 antibody functionalized CNTs stock solution. (Detailed results are provided in the Supplementary section, Fig. S-3).

### 2.5. Optimization of flow rate using biotin-streptavidin as an antibody-antigen pair

A top electrode with a channel of 800  $\mu\text{m}$  X 20 mm was attached to the biotin functionalized chip from Section 2.3 with four clamps secured at four corners, 5  $\mu\text{l}$  of the biotin functionalized CNTs was loaded into the channel. 100 V DC voltage was applied for 5 min with Keithley 2636A System SourceMeter by connecting the top electrodes and two bottom electrodes. Then an AC voltage  $V_{pp}$  value of 5 V at 5 MHz was applied for 15 min with Agilent 33220A Function/Arbitrary Waveform Generator. A syringe with 1X PBS solution was connected to the channel to shear off non-specifically bounded no-target CNTs. All current measurements were conducted at 1 V with Gamry Potentiostat 600.

### 2.6. Detection of streptavidin/HER2/HER2 in undiluted serum sample

Twenty  $\mu\text{l}$  of streptavidin/HER2/HER2 spiked serum solution was added onto functionalized chips from Section 2.3 and incubated at room temperature. After incubation, the chip was rinsed 3 times with 1X PBS to remove non-bounded targets. 10  $\mu\text{l}$  of biotin/detection HER2 antibody functionalized CNTs solution from Section 2.4 was diluted 10,000, 100,000, and 1,000,000 times with 0.1X PBS. Then the top electrode was attached to the chip, and 5  $\mu\text{l}$  of the diluted biotin/detection HER2 antibody functionalized CNTs was loaded into the channel to bridge the electrodes under DC and AC dielectrophoresis assisted deposition. After shearing at 0.5 ml/min with 1X PBS for 20 min, the current was measured at 1 V using Gamry.

## 3. Results and discussion

### 3.1. Design strategy

**Fig. 1** contains a schematic representation of the open-flow CNT on-off switch based protein detection platform that employs two major non-equilibrium steps. The first non-equilibrium step (**Fig. 1** step 2) is to bridge DNA-wrapped and detection (monoclonal) antibody-functionalized CNTs across the two electrodes. This is achieved by an irreversible assembly phenomenon, driven first by DC electrophoresis that rapidly places the CNTs vertically on top of the electrodes. Since DC field is long range with high electric fields, a majority of the negatively charged CNTs can be attracted to the electrodes within one minute. Their electrostatic repulsion sustains equal spacing between the vertically aligned CNTs along the DC field lines. Then AC DEP is activated to quickly align the CNTs horizontally, resulting in bridging of the two electrodes and formation of the Ab-Ag-Ab CNT complexes. The bridged CNTs transform the system into a switch-on mode and conduct current by CNT electron tunneling. The second non-equilibrium step (**Fig. 1** step 3) is to improve the selectivity of detection by hydrodynamic shearing. Because of the large hydrodynamic drag imposed by a cross-flow on cylindrical CNTs with high aspect ratio, we can selectively remove non-target or no-target bound CNTs under a critical flow shear rate. The remaining aligned target-antibody bound CNTs will produce current signals that will be correlated with the target (CNT) number.

### 3.2. Rapid and efficient alignment of the CNTs with DC and AC DEP

Preliminary studies were conducted on parallel clean Au electrodes with 3  $\mu\text{m}$  gap to test CNTs alignment by using the sequential DC and AC DEP protocol. **Fig. 2a** illustrates the schematics of switch on and off states, where CNTs act as current reporters. The SEM image (II) in **Fig. 2a** further confirms the presence of CNTs alignments at switch-on state. It is clear to see that most of CNTs align in parallel bridging across the electrodes without aggregation, and any small aggregations near the edge of the electrodes are due to the evaporation of the

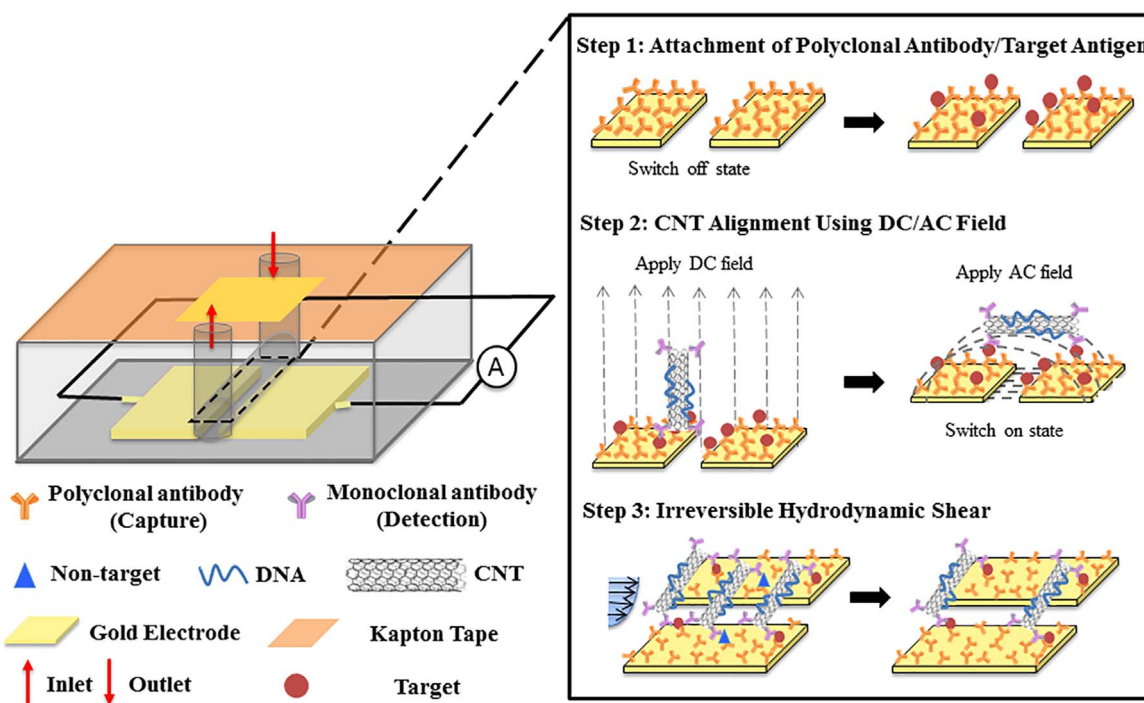


**Fig. 1.** The schematic of one-dimensional CNTs switch sensor for protein detection. Step1: Targets incubated with polyclonal antibodies. Step 2: CNTs assembly with DC electrophoresis at 100 V for 5 min and then AC DEP at 10 V, 5 MHz for 15 min. Step 3: 1X PBS solution shearing at 0.5 ml/min to irreversibly remove non-specific CNTs binding.

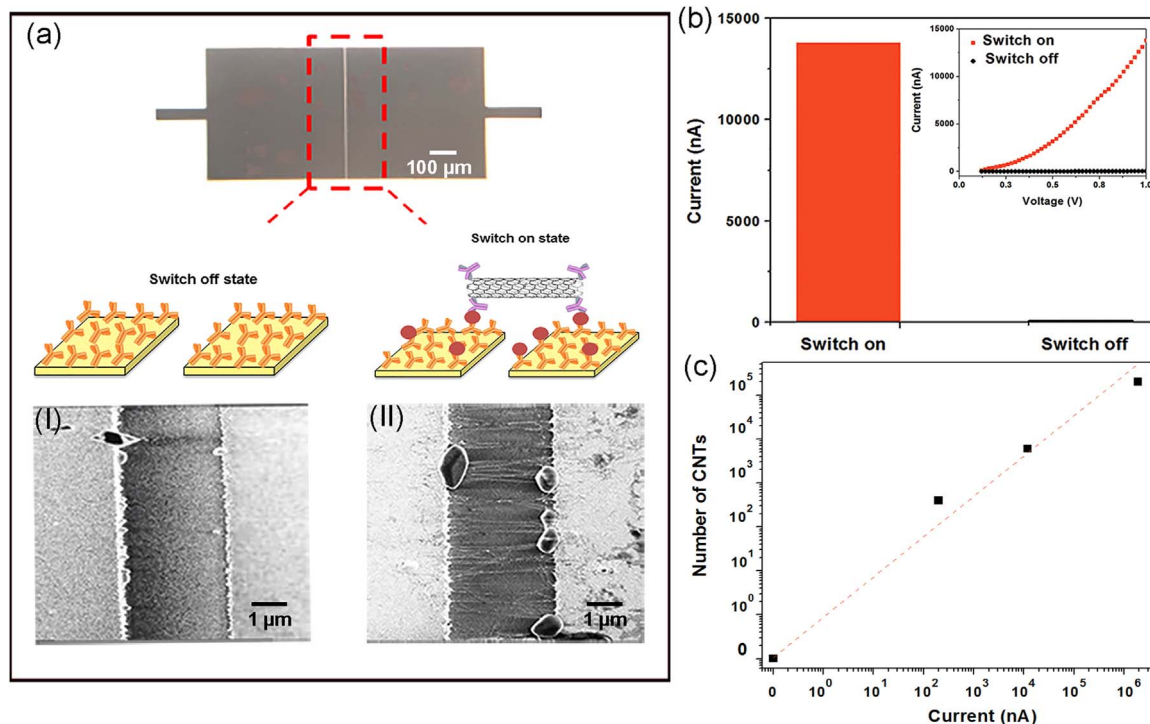


**Fig. 2.** CNTs act as switches to connect gold electrodes to produce current signal. (a) A schematic of switch-on state with CNTs and switch-off state; Inset of Fig (a) shows the respective SEM images (I-II) of no-CNTs at switch off state and aligned CNTs at switch on state. The chips were imaged by a Carl Zeiss EVO-50 SEM. (b) Currents for switch-off (black column) state and switch-on (red column) state at 1 V. Inset of (b) shows the current measurements for switch-on (red) and switch-off (black) states under increasing voltage from 0 to 1 V, respectively. (c) A correlation between current signal with respective to CNT numbers under DC/AC DEP deposition. Measurements were conducted in 1X PBS solution at 1 V. (For interpretation of the references to color in this figure legend, the reader is referred to the web version of this article.)

solvents before imaging. The well aligned CNTs at switch-on state produce a current signal that is 5 orders of magnitude more than that of the switch off state (Fig. 2b) at 1 V. Such a large current differences demonstrate highly sensitive and effective conductance between CNTs and electrodes at the switch on state. It is also important to note that such a big current difference contributes to a very low and stable baseline current at the switch-off state when there are no CNTs bridging (SEM (I)). This is because the current is exclusively carried by CNTs bridging, without measurable parasitic currents from electrochemical reactions at the electrodes. As a result, the baseline current is negligibly small at the absence of CNTs and remains inert to different pH, buffer ionic strength or the types of buffer solutions. Since the bridged CNTs had such good alignments, the number of CNTs bridged was easily estimated and plotted against the corresponding current illustrated in Fig. 2c. Fig. 2c shows a linear relationship between the current and the number of CNTs aligned, with a correlation coefficient of 0.99 from the linear regression. Extrapolating our data to one CNT, the theoretical detection limit can hence go down to aM to fM if there are, on the average, 2–2000 numbers of antigens on a single carbon nanotube with 10 μl of sample volume, including ones on the electrodes that have not formed complexes with the CNT. The dynamic range also goes up to 6 orders of magnitude, and can be further expanded by decreasing gap size, and increasing the polyclonal antibody density on gold electrode and the number of CNTs deposited. The low detection limit and large dynamic range of this platform would then allow us to detect a wide range of protein biomarkers with different concentrations. (Additional optimization of applied voltage and CNT alignment results are discussed in the Supplementary section, S1).

### 3.3. Platform performance against low dissociation constant biotin and streptavidin pairs

In order to examine the feasibility of the platform and its sensitivity

and selectivity, we used a streptavidin and biotin pair as a model system. Biotin and streptavidin pairs have very strong binding affinity compared with antigen-antibody pairs in real clinical sample (Allen et al., 1997; Hu et al., 2007). The dissociation constant for biotin and streptavidin is 10 fM (Holmberg et al., 2005), and bonds are stable through a wide range of pH and temperature. We used biotin as both capture antibody and detection antibody, and pure streptavidin were used as target. As the used CNTs are of 1–3 μm, for sensing study we fabricated chips with 1 μm gap in order to have 100% of CNTs bridging. To demonstrate that hydrodynamic shear is selective towards target streptavidin, the experiments were designed on chips with and without streptavidin (Fig. 3a). It is expected that after biotin functionalized CNTs are aligned, flow will irreversibly remove any CNTs that have not bound to any streptavidin. Fig. 3b has confirmed that under the same CNTs deposition, a flow rate at 0.5 ml/min can remove more than 99% of the CNTs when no streptavidin is incubated. When streptavidin is incubated, the targets are able to hold CNTs on the electrodes with strong binding forces to withstand the drag force exerted on the CNTs under shear. Moreover, Fig. 3b indicates that the higher concentration of streptavidin incubates, the more target antibody CNT complexes form to produce higher current. Thus, it is fair to conclude that flow shearing can selectively remove no-target bound CNTs. It should be noted that the selectivity is directly related to the flow shear rate, and a high shear rate can remove both no-target and target bound CNTs, so it is important to optimize shear rate in order to achieve high selectivity. At the same time, the number of CNTs needs to be well selected so that the antibody probes on the CNTs are higher than the number of targets to avoid target saturation. In fact, by optimizing the number of CNTs with respect to target concentrations, the dynamic range can be linearly extended without target saturation (More results are discussed in Supplementary section S4, Fig. S-4). So with the optimal number of CNTs, we established the calibration curve in Fig. 3c for the 100 aM to 1 pM range of a pure streptavidin sample. For each concentration,

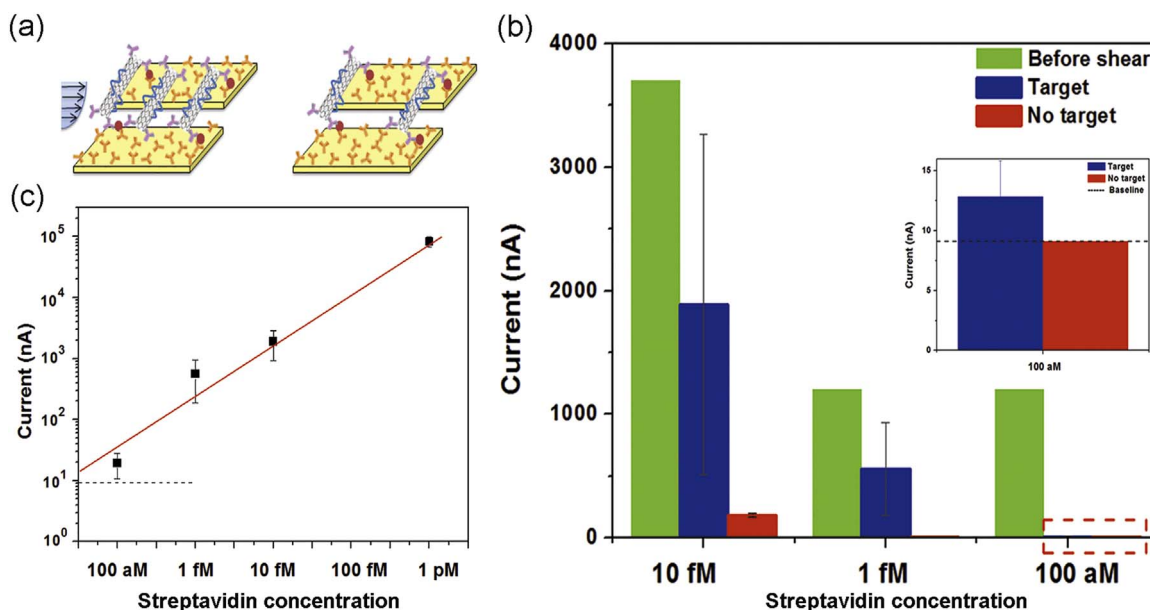


**Fig. 3.** The platform is highly sensitive and selective toward streptavidin with irreversible shear. (a) The schematic of irreversible shear with target bound CNTs and no-target bound CNTs. (b) Selectivity results of target (blue column) and no-target (red column) incubation after irreversible shearing. Under the same CNTs deposition (green column) before shearing, only the target streptavidin bound CNTs are able to hold CNTs and produce current signals higher than the baseline current (black dotted line). A blow up plot of target and no-target after shear for 100 aM concentration is shown as an inset in (b). (c) The calibration curve of the streptavidin concentration, where the detection limit is 100 aM, and the baseline current for 100 aM and 1 fM is shown. The dynamic range is 5 orders of magnitude. (For interpretation of the references to color in this figure legend, the reader is referred to the web version of this article.)

samples are tested on multiple chips to confirm reproducibility. The graph reveals a linear regime from 100 aM to 1 pM with a correlation coefficient of 0.97 from linear regression. The limit of detection is determined when the detected current value of the target concentration is equal to 3 standard deviations of the baseline current, which measures the data variation over multiple chips. For biotin and streptavidin pair, a detection limit of 100 aM is 2 orders of magnitude lower than the dissociation constant for biotin and streptavidin pair. At 100 aM concentration, there is about 10 CNTs bridging across the electrodes based on the linear correlation from Fig. 2c, and the numbers of targets on each of CNTs are around 20 assuming all streptavidin bind. Such a low detection limit is a result of sensitive CNTs electron tunneling at switch-on state, and the low baseline current and noise level at switch-off state, where there is no CNTs or electrochemical reactions to contribute to current. The linear calibration curve indicates a dynamic range that could be 5 orders of magnitude more if higher streptavidin concentrations are measured. In all, biotin and streptavidin detection has shown that the platform is sensitive and selective toward targets with CNTs concentrations optimized for target concentrations.

#### 3.4. Platform performance against high dissociation constant HER2 and HER2 antibody pairs

In order to evaluate the sensitivity and selectivity of the platform against real protein and antibody pairs which usually have higher dissociation constants, a breast cancer biomarker HER2 and HER2 antibody pair is selected. HER2 is an important biomarker for breast cancer, and its status is routinely assessed when breast cancer is diagnosed. An overexpression of HER2 is a significant predictor of reduced survival rate and shorter time to elapse (Berghoff et al., 2014). The  $K_D$  of HER2 and its antibody is around  $0.44 \pm 0.07$  nM (Zhang et al., 2011), so it is more challenging to detect HER2 at lower concentrations. We first tested with pure HER2 samples to find the detection limit and dynamic range for this low binding affinity pair. The

calibration curve was developed in Fig. 4b from 10 fM to 100 pM. The graph reveals a linear regime for all measured target concentrations on multiple chips with a correlation coefficient of 0.989. As illustrated, the detection limit is 10 fM, which is higher than that of the biotin and streptavidin model. This is expected since the dissociation constant of HER2 is 10,000 times higher than that of biotin and streptavidin, so only at higher concentrations of incubated targets can form efficient Ab-Ag complexes to hold the CNTs against the drag force during flow shearing. Nevertheless, it is important to note that 10 fM of detection limit is 4 orders of magnitude lower than its  $K_D$  value, which is a result of DC and AC DEP CNT deposition technique that facilitates the formation of Ab-Ag complex at much lower target concentration. This study clearly demonstrates that the platform is highly sensitive with a dynamic range up to 5 orders of magnitude.

A stringent selectivity test was done with a HER2 isoform as the non-target negative control (Fig. 4a). This HER2 isoform is a partial recombinant protein that binds to the detection antibody with the same binding affinity as the target HER2. However, it binds to the capture antibody with less affinity. Fig. 4c illustrates that the flow shearing removes more than 95% of the HER2 isoform non-targets bound CNTs. But HER2 bound CNTs complex are able to stand the shearing step with a current that is 1000 times higher than that of the non-target HER2. It is important to note that the concentration of the non-target HER2 isoform is 1 nM, which is 100 times higher than target concentration of 10 pM, indicating an effective shear-enhance discrimination of non-targets by a factor of several orders of magnitude. To further validate the sensor's selectivity performance, a mixture of 10 pM target and 1 nM non-target sample was tested. Despite the presence of 100 times more non-targets, the current value is still 3 orders of magnitude higher than that of the non-target isoform sample (Fig. 4c). The current of mixture sample is slightly less than that of pure target samples due to site competitions between targets and non-targets. In all, HER2 detection further confirms that the flow shearing is highly selective towards targets despite the presence of non-targets with high concentration.

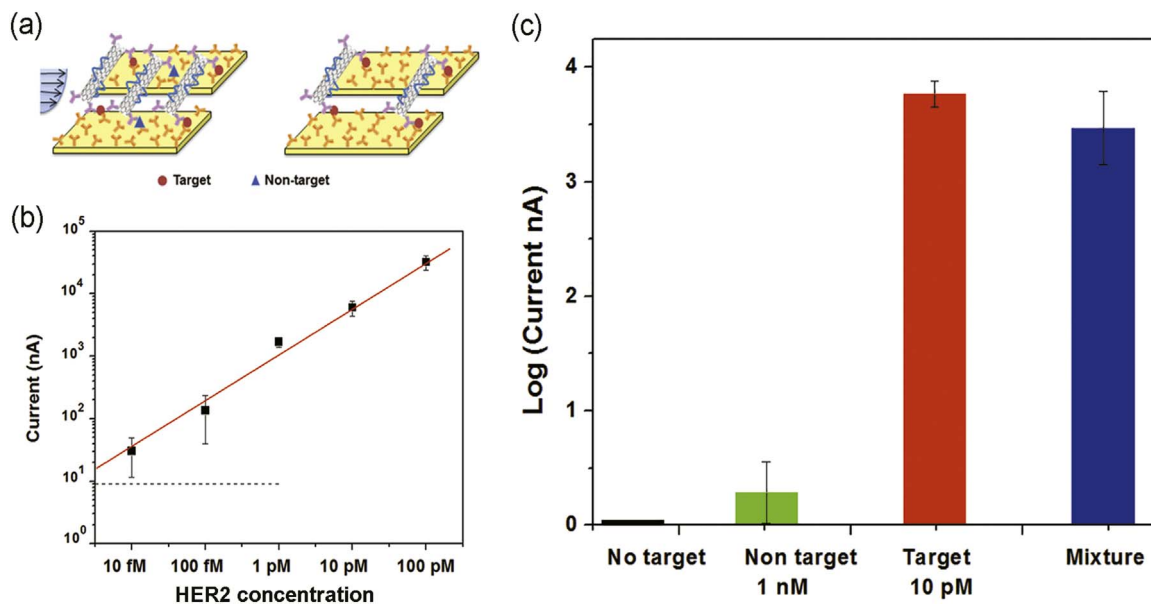


**Fig. 4.** The platform is highly selective toward HER2 with irreversible shear. (a) The schematic of irreversible shear with target bound CNTs and non-target bound CNTs. Only the non-target bound CNTs are removed by irreversible flow. (b) The calibration curve of different HER2 concentrations, where the detection limit is  $10 \text{ fM}$ , and the baseline current for  $10 \text{ fM}$  and  $1 \text{ pM}$  is shown. The dynamic range is 5 orders of magnitude. (c) Selectivity results of no-target (black column), target HER2 (red column), non-target HER2 isoform (green column) and a mixture of target HER2 and non-target (blue column) incubation after irreversible shearing. (For interpretation of the references to color in this figure legend, the reader is referred to the web version of this article.)

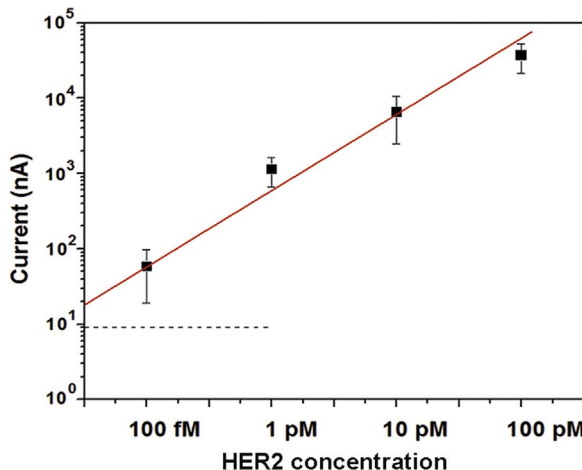


**Fig. 5.** Detection of HER2 spiked in human serum. The calibration curve of different HER2 concentrations in undiluted serum sample, where the detection limit is lower than  $100 \text{ fM}$ , and the dynamic range is 4 orders of magnitude.

### 3.5. Platform performance against HER2 serum samples

We have further validated the performance of the platform with a heterogeneous sample. In this study, we selected four different concentrations of HER2 targets and spiked them into undiluted human serum. Measurements were also conducted with only human serum to create a baseline with different CNTs concentrations to eliminate the effect of pre-existing HER2 in serum (Fig. S-5). A calibration curve was developed and presented in Fig. 5. The graph reveals a linear regime for all measured target concentrations with a correlation coefficient of 0.98. At a  $100 \text{ fM}$  concentration, the detected current is well above the 3 standard deviations of the baseline current, indicating a detection limit lower than  $100 \text{ fM}$ . Nevertheless,  $100 \text{ fM}$  of detection is already 3 orders of magnitude lower than the dissociation constant of HER2 and its antibody pair. Since human serum has a high abundance of non-target proteins that could potentially compete with targets for complex association with antibodies. This makes the detection sensitivity one

order of magnitude lower than that of pure sample. However, a detection of  $100 \text{ fM}$  is still better than the limit of any commercially available HER2 ELISA kit. At the same time, the detection dynamic range is 4 orders of magnitude, and this value can continue to increase for higher concentration target detection based on the linearity of the calibration curve.

### 4. Conclusions

We developed a very sensitive, selective and quantifiable CNT-ELISA platform for protein detection, which assembles individual antibody functionalized CNTs to bridge across the electrodes to bind with targets. The CNTs serve both as a transporter and a reporter for the target-linker. The key step is the DC electrophoresis and AC dielectrophoresis assisted deposition and assembly that helps to achieve rapid CNTs deposition while facilitates target and antibody binding by bringing them closer. The use of 1X PBS hydrodynamic shearing produces enhanced drag force on the CNTs that irreversibly removes no-targets or non-targets, elevating the selectivity beyond the thermodynamic limits. As a result, we potentially improved the performance of conventional ELISA assay by sub-fM detection limit (2 orders improvement) and 4-decade dynamic range (1 or 2 orders improvement) for HER2 serum sample by scaling the initial CNTs concentrations with the target concentrations. There are many variables that can be studied systematically in order to further lower the detection limit, improve the selectivity as well as decrease assay time. For instance, DC and AC dielectrophoresis field strengths, target incubation time, shearing buffer efficacy, electrode area, CNT concentrations etc. We will also scale up the platform to multi-target sensing by incorporating different antibody functionalized CNTs in multiple parallel channels. The high sensitivity and selectivity and linear detection signal output render the platform very attractive for commercialization. As the device requires imprinted gold electrodes, the cost per test will be higher than the commercially available ELISA dipstick kits, like the pregnancy test which costs less than \$1 per test, which have much lower sensitivity. However, from our commercialization experience for a similar micro-electrode sensor with FCubed LLC, we expect the cost to be significantly lower than current ultra-sensitive

immune-assay platforms with comparable sensitivity, such as Reverse Phase Protein Array (RPPA) which costs \$ 750 per sample set from MD Anderson Cancer center (Hennessy et al., 2010). We estimate a cost of around US\$20 per test, with the actual cost being mostly determined by the electrode-printing manufacturing process.

## Acknowledgement

We would like to thank Prof. Laurie Littlepage of Harper Cancer Research Institute and Department of Chemistry and Biochemistry of University of Notre Dame for valuable discussion regarding the selection of proper breast cancer biomarker. This work was supported by National Institutes of Health [1R21CA206904-01 (Hsueh-Chia Chang and Satyajyoti Senapati)]; and National Institutes of Health [1R21AI105361-01 A1 (Satyajyoti Senapati)].

## Appendix A. Supplementary material

Supplementary data associated with this article can be found in the online version at <http://dx.doi.org/10.1016/j.bios.2017.05.053>.

## References

- Allen, S., Chen, X., Davies, J., Davies, M.C., Dawkes, A.C., Edwards, J.C., Roberts, C.J., Sefton, J., Tendler, S.J.B., Williams, P.M., 1997. *Biochemistry* 36 (24), 7457–7463.
- Anderson, L., 2005. *J. Physiol.* 563 (Pt 1), 23–60.
- Balasubramanian, K., Burghard, M., 2006. *Anal. Bioanal. Chem.* 385 (3), 452–468.
- Basuray, S., Senapati, S., Aijian, A., Mahon, A.R., Chang, H.C., 2009. *ACS Nano* 3 (7), 1823–1830.
- Berghoff, A.S., Bartsch, R., Preusser, M., Ricken, G., Steger, G.G., Bago-Horvath, Z., Rudas, M., Streubel, B., Dubsky, P., Gnant, M., Fitzal, F., Zielinski, C.C., Birner, P., 2014. *Breast* 23 (5), 637–643.
- Bruno, R.D., Njar, V.C., 2007. *Bioorg. Med. Chem.* 15 (15), 5047–5060.
- Budman, L.I., Kassouf, W., Steinberg, J.R., 2008. *Can. Urol. Assoc. J.* 2 (3), 212–221.
- Cheng, I.F., Senapati, S., Cheng, X., Basuray, S., Chang, H.C., Chang, H.C., 2010. *Lab Chip* 10 (7), 828–831.
- Chikkaveeraiah, B.V., Bhirde, A.A., Morgan, N.Y., Eden, H.S., Chen, X., 2012. *ACS Nano* 6 (8), 6546–6561.
- Findlay, J.W., Smith, W.C., Lee, J.W., Nordblom, G.D., Das, I., DeSilva, B.S., Khan, M.N., Bowsher, R.R., 2000. *J. Pharm. Biomed. Anal.* 21 (6), 1249–1273.
- Gam, L.H., 2012. *WJEM* 2 (5), 86–91.
- Glaser, R.W., 1993. *Anal. Biochem.* 213 (1), 152–161.
- Gomes-Filho, S.L.R., Dias, A.C.M.S., Silva, M.M.S., Silva, B.V.M., Dutra, R.F., 2013. *Microchem. J.* 109, 10–15.
- Grieshaber, D., MacKenzie, R., Voros, J., Reimhult, E., 2008. *Sensors* 8 (3), 1400–1458.
- Hennessy, B.T., et al., 2010. *Clin. Proteom.* 6 (4), 129–151.
- Holmberg, A., Blomstergren, A., Nord, O., Lukacs, M., Lundeberg, J., Uhlen, M., 2005. *Electrophoresis* 26 (3), 501–510.
- Hölzer, A., Sommerfeld, M., 2008. *Powder Technol.* 184 (3), 361–365.
- Hortin, G.L., Sviridov, D., 2010. *J. Proteom.* 73 (3), 629–636.
- Hu, G., Gao, Y., Li, D., 2007. *Biosens. Bioelectron.* 22 (7), 1403–1409.
- Jia, C.-P., Zhong, X.-Q., Hua, B., Liu, M.-Y., Jing, F.-X., Lou, X.-H., Yao, S.-H., Xiang, J.-Q., Jin, Q.-H., Zhao, J.-L., 2009. *Biosens. Bioelectron.* 24 (9), 2836–2841.
- Kitano, H., 2002. *Science* 295 (5560), 1662–1664.
- Kohno, M., Tanimura, S., Ozaki, K., 2011. *Biol. Pharm. Bull.* 34 (12), 1781–1784.
- Kokkinos, C., Economou, A., Prodromidis, M.I., 2016. *TrAC* 79, 88–105.
- Lilja, H., Ulmert, D., Vickers, A.J., 2008. *Cancer* 8 (4), 268–278.
- Maehashi, K., Katsura, T., Kerman, K., Takamura, Y., Matsumoto, K., Tamiya, E., 2007. *Anal. Chem.* 79 (2), 782–787.
- Pandiaraj, M., Sethy, N.K., Bhargava, K., Kameswararao, V., Karunakaran, C., 2014. *Biosens. Bioelectron.* 54, 115–121.
- Pei, X., Zhang, B., Tang, J., Liu, B., Lai, W., Tang, D., 2013. *Anal. Chim. Acta* 758, 1–18.
- Privett, B.J., Shin, J.H., Schoenfisch, M.H., 2010. *Anal. Chem.* 82 (12), 4723–4741.
- Rusling, J.F., Kumar, C.V., Gutkind, J.S., Patel, V., 2010. *Analyst* 135 (10), 2496–2511.
- Srinivas, P.R., Kramer, B.S., Srivastava, S., 2001. *Lancet Oncol.* 2 (11), 698–704.
- Stern, E., Wagner, R., Sigworth, F.J., Breaker, R., Fahmy, T.M., Reed, M.A., 2007. *Nano Lett.* 7 (11), 3405–3409.
- Zhang, N., Liu, L., Dumitru, C.D., Cummings, N.R., Cukan, M., Jiang, Y., Li, Y., Li, F., Mitchell, T., Mallem, M.R., Ou, Y., Patel, R.N., Vo, K., Wang, H., Burnina, I., Choi, B.K., Huber, H.E., Stadheim, T.A., Zha, D., 2011. *mAbs* 3 (3), 289–298.
- Zhang, Y., Li, J., Wang, Z., Ma, H., Wu, D., Cheng, Q., Wei, Q., 2016. *Sci. Rep.* 6, 23391.
- Zhou, R., Chang, H.-C., Protasenko, V., Kuno, M., Singh, A.K., Jena, D., Xing, H., 2007. *J. Appl. Phys.* 101 (7), 073704.
- Zhou, R., Wang, P., Chang, H.C., 2006. *Electrophoresis* 27 (7), 1376–1385.
- Zhu, C., Yang, G., Li, H., Du, D., Lin, Y., 2015. *Anal. Chem.* 87 (1), 230–249.